

# Chirpy3D: Creative Fine-grained 3D Object Fabrication via Part Sampling

Kam Woh Ng<sup>1</sup> Jing Yang<sup>2</sup> Jia Wei Sii<sup>3</sup>  
 Jiankang Deng<sup>4</sup> Chee Seng Chan<sup>3</sup> Yi-Zhe Song<sup>1</sup> Tao Xiang<sup>1</sup> Xiatian Zhu<sup>1</sup>

<sup>1</sup>University of Surrey <sup>2</sup>University of Cambridge <sup>3</sup>Universiti Malaya <sup>4</sup>Imperial College London



Figure 1. Novel, creative species created by our Chirpy3D. Feel free to name them!

## Abstract

We present Chirpy3D, a novel approach for fine-grained 3D object generation, tackling the challenging task of synthesizing creative 3D objects in a zero-shot setting, with access only to unposed 2D images of seen categories. Without structured supervision — such as camera poses, 3D part annotations, or object-specific labels — the model must infer plausible 3D structures, capture fine-grained details, and generalize to novel objects using only category-level labels from seen categories. To address this, Chirpy3D introduces a multi-view diffusion model that decomposes training objects into anchor parts in an unsupervised manner, representing the latent space of both seen and unseen parts as continuous distributions. This allows smooth interpolation and flexible recombination of parts to generate entirely new objects with species-specific details. A self-supervised feature consistency loss further ensures structural and semantic coherence. The result is the first system capable of generating entirely novel 3D objects with species-specific fine-grained details through flexible part sampling and composition. Our experiments demonstrate that Chirpy3D surpasses existing methods in generating creative 3D objects with higher quality and fine-grained details.

## 1. Introduction

This paper tackles the problem of *fine-grained* and *creative* 3D object generation. We advance beyond existing methods in both what we define as “fine-grained” — the ability to capture intricate, species-specific part details — and what we define as “creative” — the ability to generate entirely novel objects beyond those seen during training. Current approaches either reconstruct existing objects without any creativity [2, 18, 56], produce coarse 3D objects lacking fine-grained details [24, 45], break a scene into multiple objects without fine-grained control [1], generate creative objects only in 2D [35], or mix embeddings to produce novel object designs in a more abstract manner [28, 40]. In contrast, we push all boundaries simultaneously: generating entirely new, never-before-seen 3D objects while preserving species-specific, fine-grained details. For the first time, our method can generate novel 3D birds that do not exist in the real world, as illustrated in Fig. 1.

This task is particularly challenging due to its highly under-constrained nature. The model is given only unposed 2D images from seen categories, with no access to camera poses, part annotations, or object-level supervision. From this limited data, the model must infer plausible 3D structures, predict consistent multi-view geometry, and capture

fine-grained, species-specific part details — all using only category-level appearance priors. Beyond reconstructing variations of seen objects, the zero-shot requirement imposes an even greater challenge: the model must generalize to entirely novel species, which may feature unseen part combinations, novel part shapes, and attributes not observed in the training set. These compounded challenges require the model to jointly reason over the underlying part space, discover plausible object compositions, enforce structural and geometric coherence across views, and capture species-level fine-grained diversity — all without explicit part annotations, object-level correspondences, or 3D supervision.

To address these challenges, we introduce **Chirpy3D**, a novel multi-view diffusion model that decomposes training objects into anchor parts in an unsupervised manner. These object parts are modeled as a continuous distribution in a shared latent space, capturing natural variations across all parts within and across species. This distributional formulation enables smooth interpolation between anchor parts and flexible part recombination, allowing the synthesis of entirely novel objects with coherent species-specific details. A self-supervised feature consistency loss further ensures structural and semantic coherence, enforcing cross-view consistency and improving the quality and realism of unseen parts.

Our **contributions** are threefold: (1) We present a challenging yet practical problem — creating creative fine-grained 3D objects using only unposed 2D images from seen categories. (2) We propose a novel multi-view diffusion framework, Chirpy3D, for creative 3D generation via unsupervised object part decomposition and distributional modeling, enabling interpolation and flexible recombination of parts to synthesize entirely novel objects. (3) Extensive experiments demonstrate that Chirpy3D produces high-quality 3D objects with unprecedented fine-grained detail and creative flexibility.

## 2. Related work

**Fine-grained generation.** Research on fine-grained visual understanding has primarily focused on 2D tasks, including fine-grained recognition [5, 10, 34, 51, 57] and 2D object generation [6, 9, 29, 30, 47, 54]. In contrast, fine-grained 3D generation remains underexplored, with most existing works focusing on relatively simple, rigid categories such as chairs and cars [13, 15, 16, 23, 37, 46, 55]. Deformable fine-grained categories, such as birds and dogs, pose unique challenges due to their complex textures, diverse part configurations, and high pose variability — all while obtaining high-quality 3D data for these categories remains expensive and impractical. Our work pushes beyond these limitations to enable the creative synthesis of novel, fine-grained 3D objects directly from unposed 2D images.

**Diffusion models.** Diffusion models have recently been

applied to multi-view generation, though they often suffer from multi-view inconsistencies — commonly known as the “Janus problem.” Text-to-multi-view methods such as MVDream [45] and SPaD [24] generate object views from text prompts, while methods like Zero123 [31], Zero123++ [44], and EscherNet [26] infer novel views from a single image. These methods focus on rendering consistent views of known objects, but they lack the capability to model fine-grained part-level variations or support the creative generation of novel objects. Our approach extends this line of work by enabling the generation of entirely new fine-grained 3D objects in a zero-shot setting, including novel part combinations and species-level diversity.

**Part-aware object generation.** Part-aware generation has been extensively explored in 2D, where methods such as Break-A-Scene [1] and PartCraft [35] leverage attention-based objectives to disentangle and recombine object parts. In 3D, part-aware generation has largely been confined to synthetic datasets with explicit part annotations, such as ShapeNet [4], making these approaches poorly suited for fine-grained, deformable objects [20, 27, 37, 52]. We break these limitations by enabling the creative generation of deformable fine-grained 3D objects without any part annotations or 3D supervision, discovering parts in an unsupervised manner and modeling them as continuous distributions for flexible recombination.

**Novel object creation.** The creative synthesis of novel objects has been explored through approaches based on GANs [11, 14, 36, 43] and VAEs [7, 8], which synthesize new objects by combining components from existing ones. More recently, Concept Decomposition [49] proposed a diffusion-based framework for recombining fine-grained elements, while ConceptLab [40] and TP2O [28] explored mixing embeddings to generate novel object designs. Our work advances this direction by enabling creative synthesis of entirely new fine-grained 3D objects, achieved by discovering, modeling, and sampling parts — all without part-level supervision or object-specific 3D data.

## 3. Methodology

### 3.1. Overview

Our goal is to generate fine-grained and creative 3D objects in a zero-shot setting, using only unposed 2D images from seen fine-grained categories (e.g., bird species) as training data — without part annotations, camera poses, or object-level supervision. This requires the final model to infer plausible 3D structures, discover meaningful object parts, capture species-specific fine-grained details, and generalize to entirely novel species with unseen part combinations.

To achieve this, we propose **Chirpy3D** (see Figure 2), a multi-view diffusion framework that learns a *hierarchical part latent space*, where both species-level and part-level in-

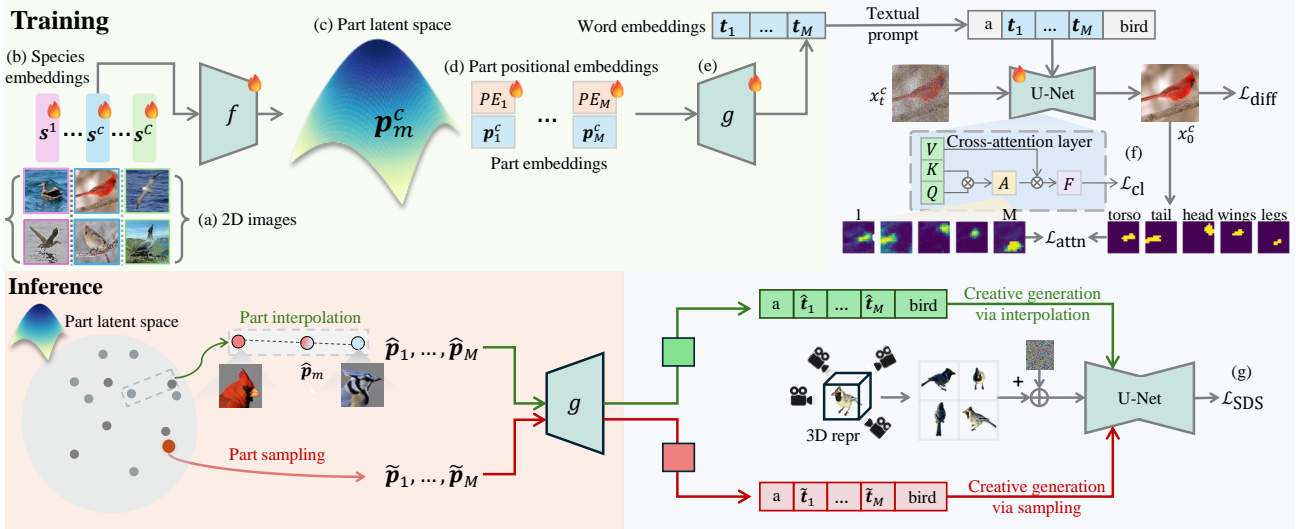


Figure 2. Overview of **Chirpy3D**. Chirpy3D takes (a) a set of unposed 2D images from multiple fine-grained species (e.g., birds) and (b) learns to decompose each object into a set of underlying parts (e.g., head, wings, torso, legs, tail) within a hierarchical part latent space – species embedding  $s$  captures global species characteristics while part-level embedding  $p$  captures fine-grained part variations. (c) A regularized part latent space ensures smooth interpolation and novel part synthesis via a standard Gaussian prior, enabling creative generation through flexible part recombination. (d) Part-specific position embeddings ( $PE$ ) are shared across all categories, enabling cross-species part alignment. (e) Part embeddings are projected via a learnable function  $g$  into part-aware textual embeddings to condition the multi-view diffusion model (e.g., MVDream [45]) to generate multi-view images. (f) A self-supervised feature consistency loss is applied to enforce structural and semantic coherence across views, improving the realism and alignment of both seen and unseen parts. (g) During inference, Chirpy3D supports both reconstruction and creative generation – either directly using learned part latent codes or sampling/interpolating within the part latent space – which guides 3D representation learning (e.g., NeRF or 3DGS) via SDS optimization.

formation are represented in a structured and compositional manner. To leverage the rich generative prior of pre-trained diffusion models, these part embeddings are projected into a space compatible with an off-the-shelf multi-view diffusion model (e.g., MVDream [45]), enabling more effective learning of the part latent space through consistent multi-view generation. This hierarchical design enables the model to not only reconstruct objects from seen species, but also compose novel objects with entirely new part synthesis and recombination.

### 3.2. Hierarchical part latent space

Chirpy3D decomposes each object into a set of  $M$  parts (e.g.,  $M = 5$  for head, wings, torso, legs, tail) in an unsupervised manner. For a dataset covering  $C$  species, we have species-level embeddings  $\{s^c \in \mathbb{R}^{D_s}\}_{c=1}^C$  and part embeddings for each species  $\{p_m^c \in \mathbb{R}^{D_p}\}_{m=1}^M = p^c$ . For each image  $x^c$  of species  $c$ , the species-level embedding  $s^c$  is projected through a learnable function  $f$  to produce the part embeddings  $\{p_m^c\}_{m=1}^M$ .

To encourage smooth interpolation and enable sampling of entirely new parts, these part embeddings are regularized to follow a standard Gaussian distribution:

$$\mathcal{L}_{\text{reg}} = \frac{1}{\sigma^2} \mathbb{E}_{c,m} [\|p\|^2]. \quad (1)$$

To ensure consistent part representations across both seen and unseen species, Chirpy3D introduces part-specific position embeddings ( $PE$ ), which are shared across all categories. These learnable embeddings ensure that corresponding parts (e.g., wings across different species) occupy aligned locations in the latent space, facilitating cross-species part composition.

Each part embedding is concatenated with its corresponding positional embedding and projected through a second learnable function  $g$  to obtain a part-specific textual embedding:

$$\begin{aligned} p_1^c, \dots, p_M^c &= f(s^c), \\ t_m^c &= g([p_m^c, PE_m]), \quad \forall 1 \leq m \leq M, \end{aligned} \quad (2)$$

where  $PE_m \in \mathbb{R}^{D_p}$  is the learnable positional embedding for part  $m$ ,  $[\cdot, \cdot]$  denotes concatenation, and  $f$  and  $g$  are implemented as a one-layer MLP and a two-layer MLP, respectively.

### 3.3. Model optimization

To enforce part-wise disentanglement during generation, we adopt the entropy-based attention loss from [35]. This loss encourages each part textual embedding  $t_m^c$  to attend to its corresponding spatial location in the cross-attention maps

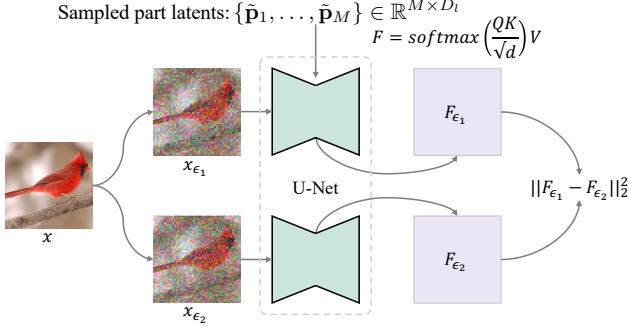


Figure 3. As we do not have images of unseen part latents, we use real natural images as our proxy. We extract cross-attention feature maps  $F$  of two noised latents, then minimize the discrepancy between the two feature maps. This will encourage the model to compute similar feature maps for any given part latents, which indirectly stabilizes the denoising process for unseen latents.

during fine-tuning of the diffusion backbone. Our objective function consists of three key components:

$$\mathcal{L}_{\text{diff}} = \mathbb{E}_{\mathbf{x}, \mathbf{y}, t, \epsilon} [\|\epsilon - \epsilon_\theta(\mathbf{z}_t; \mathbf{y}, t)\|_2^2], \quad (3)$$

$$\mathcal{L}_{\text{attn}} = \mathbb{E}_{\mathbf{z}, t, m} [-\mathbb{S}_m \log \hat{\mathbb{A}}_m], \quad (4)$$

$$\text{where } \hat{\mathbb{A}}_{m,i,j} = \frac{\bar{\mathbb{A}}_{m,i,j}}{\sum_{k=1}^M \bar{\mathbb{A}}_{k,i,j}}, \quad \bar{\mathbb{A}}_m = \frac{1}{L} \sum_l \mathbb{A}_{l,m},$$

where  $\mathcal{L}_{\text{diff}}$  is the standard diffusion loss, with  $\mathbf{z}_t$  representing the noised latent state of input  $\mathbf{x}$  at timestep  $t$  and  $\mathbf{y}$  as the text prompt like “a  $t_1^c, \dots, t_M^c$  bird”.  $\mathcal{L}_{\text{attn}}$  is the cross-entropy loss between the normalized cross-attention map of part  $m$  and its predicted binary segmentation mask  $\mathbb{S}_m$ , obtained from the part segmentation module in [35]. Here,  $\mathbb{A}_{l,m}$  represents the cross-attention map from layer  $l$ , indicating the correlation between part  $m$  and the noisy latent  $\mathbf{z}_t$ . The averaged attention map  $\bar{\mathbb{A}}_m$  aggregates attention across  $L$  selected layers, while  $\hat{\mathbb{A}}_{m,i,j}$  normalizes the attention across all  $M$  parts.

**Self-supervised feature consistency loss.** To enhance structural and semantic coherence across views, we introduce a self-supervised feature consistency loss  $\mathcal{L}_{\text{cl}}$ , which improves the visual quality and geometric consistency of both seen and novel objects. We achieve this by extracting cross-attention feature maps  $F$  from multiple layers of the network, which directly influence image content. To sample an unseen part  $m$ , we generate a latent embedding from a Gaussian distribution:

$$\tilde{\mathbf{p}}_m \sim \mathcal{N}(\boldsymbol{\mu}_m, \boldsymbol{\sigma}_m^2), \quad (5)$$

where  $\boldsymbol{\mu}_m = \frac{1}{C} \sum \mathbf{p}_m^c$  and  $\boldsymbol{\sigma}_m^2 = \frac{1}{C} \sum (\mathbf{p}_m^c - \boldsymbol{\mu}_m)^2$ . The sampled latent  $\tilde{\mathbf{p}}_m$  is then passed through  $g$  to produce a textual embedding  $\hat{\mathbf{t}}_m$ . The consistency loss  $\mathcal{L}_{\text{cl}}$  is applied to minimize the L2-distance between feature maps across

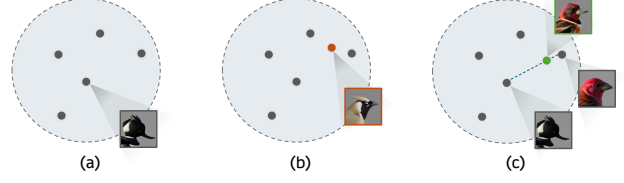


Figure 4. (a) Seen part selection generation. Unseen part synthesis via (b) novel sampling and (c) interpolation.

different noise levels:

$$\mathcal{L}_{\text{cl}} = \mathbb{E}_{t, \epsilon, L} \left[ \sum_{i,j} \|F_{\epsilon_i} - F_{\epsilon_j}\|^2 \right]. \quad (6)$$

where  $i, j$  represent different random noise inputs at the same timestep  $t$ , and  $L$  denotes different layers in the U-Net. See Figure 3 for an illustration.

**Final objective function.** The full optimization objective for Chirpy3D is:

$$\mathcal{L} = \mathcal{L}_{\text{diff}} + \lambda_{\text{attn}} \mathcal{L}_{\text{attn}} + \lambda_{\text{cl}} \mathcal{L}_{\text{cl}} + \lambda_{\text{reg}} \mathcal{L}_{\text{reg}}, \quad (7)$$

where  $\lambda_{\text{attn}} = 0.01$ ,  $\lambda_{\text{cl}} = 0.001$ , and  $\lambda_{\text{reg}} = 0.0001$  control the relative contributions of each loss term.

### 3.4. Creative object generation

**Part-aware multi-view image generation.** Chirpy3D provides flexible mechanisms for generating fine-grained and creative objects by allowing users to compose new objects from existing or novel parts. This part-aware generation enables practically endless possibilities through combinations and sampling within the learned part space. We support three primary approaches for creating objects:

- (i) *Seen part selection generation* (see Figure 4(a)) allows users to compose new objects by selecting existing parts from seen species. Users can specify a text prompt such as “a  $t_1^*, \dots, t_M^*$  bird”, where each part is selected from different species, denoted by  $*$ .
- (ii) *Unseen part synthesis via novel sampling* (see Figure 4(b)) creates new hybrid objects by directly sampling novel parts from the learned part latent space. This approach uses text prompts like “a  $\tilde{t}_1, \dots, \tilde{t}_M$  bird”, where each part  $\tilde{t}_m$  is sampled via equation 5.
- (iii) *Unseen part synthesis via interpolation* (see Figure 4(c)) generates unique hybrids by interpolating part latents from different species. Specifically, a new part latent is computed as:

$$\hat{\mathbf{t}}_m = g([a \cdot \mathbf{p}_m^{c_1} + (1 - a) \cdot \mathbf{p}_m^{c_2}, \text{PE}_m]) \quad (8)$$

where  $\hat{\mathbf{t}}_m$  denotes the decoded textual embedding of the interpolated part latent, and  $a$  controls the interpolation weight between species  $c_1$  and species  $c_2$ .

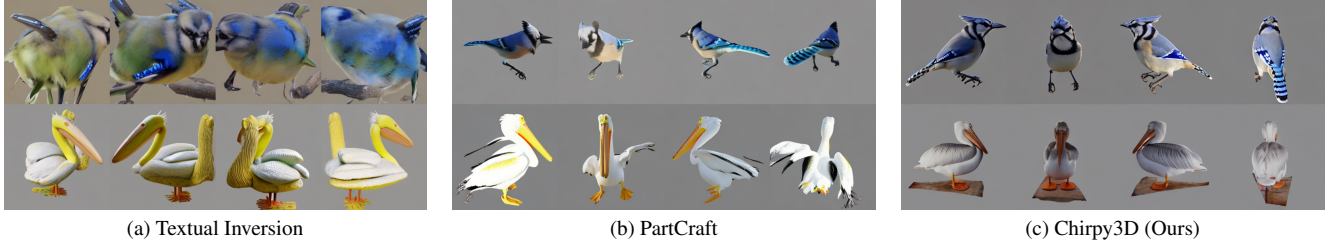


Figure 5. Multi-view subject-driven generation on two species -blue jay, white pelican. Both PartCraft and Chirpy3D achieve comparable subject fidelity, whereas Textual Inversion falls short.

**3D generation.** Chirpy3D enables the generation of complete 3D objects through Score Distillation Sampling (SDS) [38]<sup>1</sup>, supporting the three previously defined approaches. Unlike general text-to-3D generation, where broad category-level prompts like “bird” lead to diverse and often inconsistent results, Chirpy3D operates at a much finer granularity. Each textual token in Chirpy3D corresponds to a specific part from a particular species, resulting in highly consistent object appearance across different noise inputs (see Figure 12(b)). This improved consistency allows Chirpy3D to apply SDS with a lower guidance scale, reducing the risk of oversaturation (see Figure 10). Our method works effectively with both NeRF [33, 38] and 3DGS [25, 48].

## 4. Experiment

**Datasets** We conduct main experiments on the fine-grained bird dataset CUB-200-2011 [50], which consists of 5,994 training images and 5,997 test images. We use only the training set for model training. The dataset includes 200 bird species, with approximately 30 images per species.

**Implementation** All experiments were conducted on a single RTX 3090 GPU. We incorporate LoRA [21] into the cross-attention layers of the diffusion backbone, MV-Dream [45], and optimize only the LoRA parameters using single-view images. Attention loss is applied to cross-attention maps at resolutions of  $8 \times 8$  and  $16 \times 16$ . We train the model for 100 epochs using a batch size of 4 and a learning rate of 0.0001. For 3D object generation, we adopt threestudio [17] as our framework. Our setup includes a species embedding dimension of  $D_s = 768$ , a part embedding dimension of  $D_p = 4^2$ , and a text embedding dimension of  $D_t = 1024$ . The function  $f$  is implemented as a one-layer MLP, while  $g$  is a two-layer MLP.

**Competitors.** We compare Chirpy3D with two alternative models: (a) *Textual Inversion*: An adaptation of [12], which learns a set of part-specific textual embeddings. Specifically, it optimizes  $C \times M$  learnable word embeddings, where each embedding is defined as  $\mathbf{t}_m^c \in \mathbb{R}^{D_t}$ . (b)

Method	DINO $\uparrow$	CLIP $\uparrow$	FID $\downarrow$	FID <sub>CLIP</sub> $\downarrow$
Textual Inversion [12]	0.357	0.594	43.86	30.89
PartCraft [35]	0.365	0.597	<b>43.25</b>	28.98
<b>Chirpy3D</b>	<b>0.380</b>	<b>0.619</b>	43.41	<b>27.84</b>

Table 1. Results in subject fidelity metrics.

Method	EMR $\uparrow$	CoSim $\uparrow$
Textual Inversion [12]	0.210	0.691
PartCraft [35]	0.291	0.722
<b>Chirpy3D</b>	<b>0.295</b>	<b>0.724</b>

Table 2. Part composition results.

*PartCraft*: Extends (a) by incorporating a non-linear projector to further refine the learned word embeddings. For a fair comparison, all models are implemented on MVDream with rank-4 LoRA layers [21] and use attention loss  $\mathcal{L}_{\text{attn}}$  (equation 4) to enforce part disentanglement.

### 4.1. Multi-view generation evaluation

Evaluating whether a model has accurately learned to generate a subject is crucial. We assess the quality of multi-view image generation by computing the average pairwise cosine similarity between the CLIP [39]/DINO [3] embeddings of generated multi-view images (treated as four separate images) and real species-specific images. This follows the evaluation protocol proposed in [42].

Figure 5 shows that both PartCraft and Chirpy3D effectively reconstruct the subject, whereas Textual Inversion struggles to preserve fine-grained details. The subject fidelity metrics in Table 1 indicate that PartCraft and Chirpy3D achieve more comparable subject fidelity (the latter is better overall), establishing a fair baseline for further experiments. Also, we evaluate FID and FID<sub>CLIP</sub> between training and generated images, finding that Chirpy3D surpasses PartCraft by around 4% in FID<sub>CLIP</sub>.

**Part composition.** To evaluate the model’s ability to disentangle and recombine parts, we perform a *part composition* experiment, where a specific part in a target image is replaced with the corresponding part from a source image. Table 2 presents a quantitative comparison with two metrics from [35]: *Exact Matching Rate (EMR)* and *cosine similarity score (CoSim)*. See visual comparisons in Figure 6.

<sup>1</sup>We refer readers to the original paper for further details.

<sup>2</sup>We also ablate with  $D_p = 16, 32, 64$  in the supplementary material.

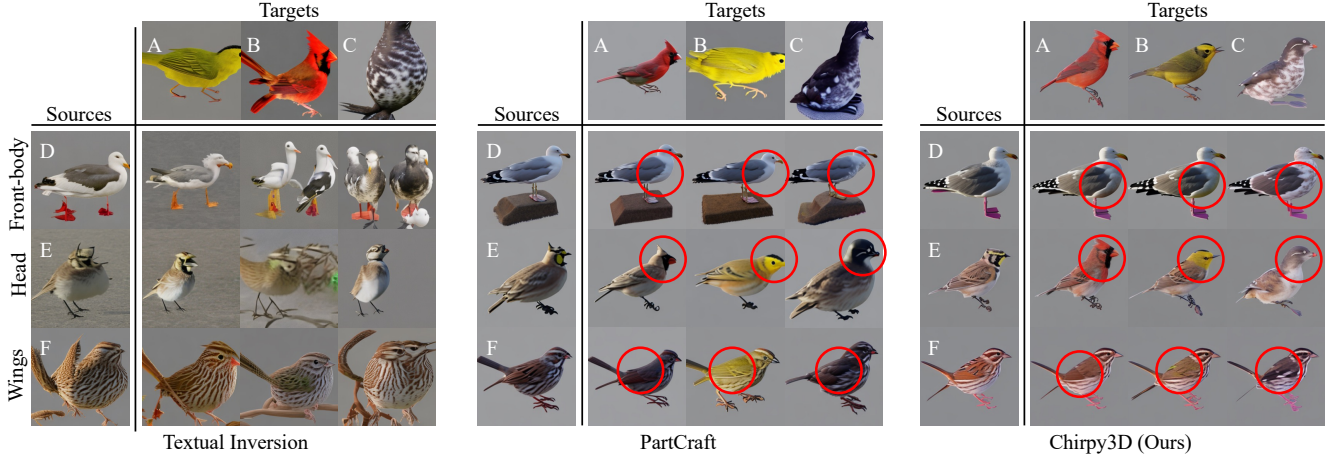


Figure 6. Visual comparison of part composition. *A, B, C, D, E, F* represent *cardinal, wilson warbler, least auklet, california gull, horned lark, and song sparrow* respectively. Red circles indicate changed parts. All generated (including sources & targets) by the same seed.

Among the methods, Textual Inversion exhibits the weakest performance, while PartCraft and Chirpy3D perform comparably. Unlike Textual Inversion, which operates directly within the textual embedding space, both PartCraft and Chirpy3D use a shared projector to map part representations into textual embeddings. This shared projection enhances part disentanglement by modeling interactions between different parts more effectively, leading to improved optimization.

**Linear interpolation.** Interpolation is a valuable tool for editing and understanding the latent space. We analyze the latent space by interpolating between latent codes and progressively generating objects from left to right, as shown in Figure 7. Our observations are as follows:

- (i) *Textual Inversion* performs poorly under interpolation. As each learned word embedding is independent, interpolating between embeddings produces out-of-distribution embeddings, leading to unnatural and glitchy images.
- (ii) *PartCraft* handles interpolation without glitches, likely due to its embedding projector, which helps establish a robust manifold of word embeddings. However, it exhibits an abrupt switching effect, where a sudden and significant change occurs at a particular interpolation step.
- (iii) *Chirpy3D* generates smooth and meaningful transitions between objects, benefiting from our distribution based *regularization loss*  $\mathcal{L}_{\text{reg}}$  (equation 1), which encourages smooth interpolation in the latent space.

**Random sampling.** To evaluate the *creativity* of different methods, we sample from the part latent space, compose novel objects, and compute two diversity measures: *entropy* ( $H$ ) and the *effective number of classes* ( $e^H$ ). These metrics compare generated samples against training data to as-

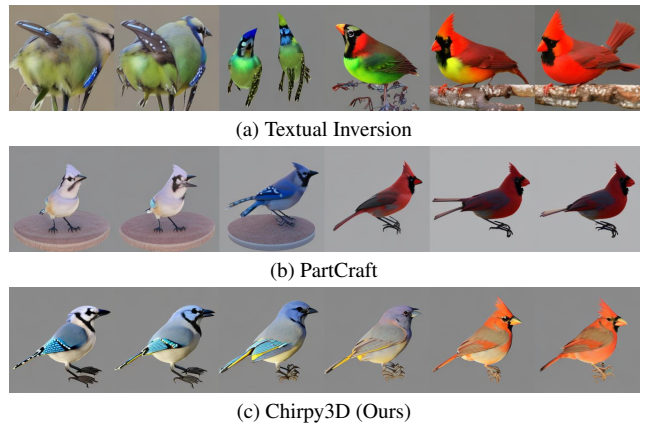


Figure 7. Linear interpolation of all part latents between two different species – *blue jay* and *cardinal*. Only one view is shown. Our Chirpy3D achieves much smoother interpolation, unlike PartCraft exhibits an abrupt switch phenomenon after a certain step (middle step).

sess how broadly or narrowly the generated objects resemble real-world species.

We begin by extracting feature embeddings from each generated multi-view image using DINO [3]. We then conduct a retrieval task, searching for the closest training images for each generated view. For each view, we retrieve the top-5 most similar species and calculate the frequency distribution of the retrieved species. To quantify diversity, we compute the *entropy* of these frequencies, where higher entropy indicates a more diverse set of generated objects. The *effective number of classes* ( $e^H$ ) provides an interpretable measure of diversity, estimating the number of classes that would appear if they were uniformly distributed. As shown in Table 3, Chirpy3D achieves a higher effective class count than PartCraft, indicating greater diversity in generating novel species.

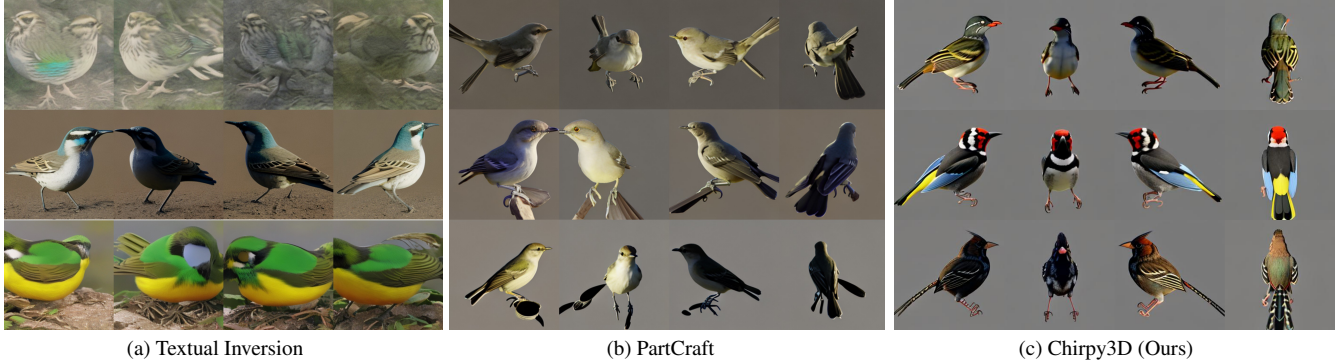


Figure 8. Generated images with random sampled latents/embeddings. Textual Inversion often produces images with artifacts due to the direct interpolation of word embeddings. PartCraft can generate images with fewer artifacts but lacks consistency. In contrast, our Chirpy3D generates novel images with greater diversity.

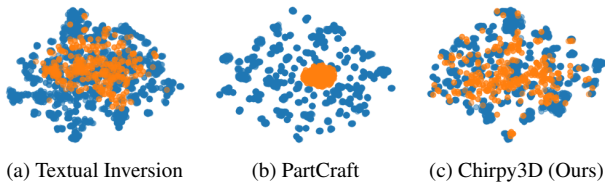


Figure 9. t-SNE embeddings of DINO features of generated images using Textual Inversion, PartCraft and Chirpy3D. **Blue** represents images of subject-driven reconstruction; **Orange** represents images of novel generation. Chirpy3D produces well-clustered DINO feature representations while also achieving a significantly broader range of diverse outputs.

Method	$H \uparrow$	$e^H \uparrow$
PartCraft [35]	4.07	58.6
<b>Chirpy3D</b>	4.81	123.2

Table 3. Diversity test. Higher values indicate greater diversity.

Qualitative results in Figures 8 and 9 further support these findings: Textual Inversion frequently produces artifacts, PartCraft generates limited class diversity (primarily brownish birds), whereas Chirpy3D yields well-clustered DINO feature representations and a significantly broader range of diverse outputs.

## 4.2. 3D generation evaluation

We present NeRF-based<sup>3</sup> subject generation, novel generation (via random sampling), and part composition in Figure 10. All generations are optimized using a standard guidance scale (*i.e.*, 7.5).

Due to the lower guidance scale, PartCraft and Textual Inversion struggle to optimize high-quality 3D objects for novel generation and part composition, often producing artifacts such as overly smooth textures and small object outputs<sup>4</sup>. Our Chirpy3D, when trained with the feature con-

<sup>3</sup>See supplementary material for 3DGS-based generation and image-to-3D methods [53].

<sup>4</sup>Increasing the guidance scale can improve 3D object quality (*e.g.*, gen-

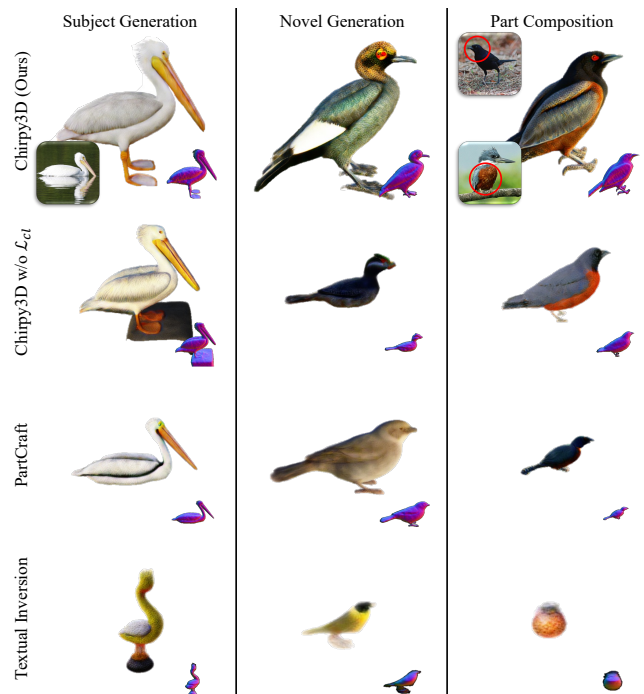


Figure 10. NeRF rendering of learned 3D objects.

Chirpy3D	With $\mathcal{L}_{cl}$	Without $\mathcal{L}_{cl}$
Preference $\uparrow$	<b>82.5%</b>	17.5%

Table 4. User study to verify  $\mathcal{L}_{cl}$ .

sistency loss  $\mathcal{L}_{cl}$ , produces significantly higher-quality 3D objects compared to the version without it, highlighting the importance of enforcing visual coherence across views.

## 4.3. Further Analysis

**Effect of  $\mathcal{L}_{cl}$ .** Since there are no training examples for unseen random samples, the model faces a significant challenge in learning how to generate realistic outputs from un-



Figure 11. **(Top)** Middle images indicate a hybrid between species/instance **left** and **right** by linearly interpolating their part latent codes. **(Bottom)** Generated images with random sampled latents for PartImageNet (quadruped only) [19] and sims4-faces [41]. We regularize part embeddings to follow a standard Gaussian distribution to encourage smooth interpolation and sampling.

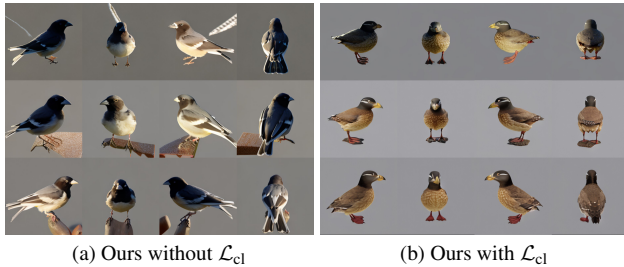


Figure 12. All images are generated with the same camera pose but with different seeds on *unseen* latent. (a) Without our feature consistency loss  $\mathcal{L}_{cl}$ , the generated images lack consistency (*e.g.*, less artifact, and inconsistent visual feature) compared to (b).

seen embeddings. Figure 12 compares our model with and without the proposed self-supervised feature consistency loss  $\mathcal{L}_{cl}$ . We observe that incorporating  $\mathcal{L}_{cl}$  significantly enhances the visual coherence of generated objects.

To further validate the impact of  $\mathcal{L}_{cl}$ , we conducted a user study to assess visual coherence. We generated 100 images (across different random seeds) for 10 existing species and 10 randomly sampled species using models with and without  $\mathcal{L}_{cl}$ . We then asked 20 users to vote for their preferred images. As shown in Table 4, 82.5% of users favored images generated by the model with  $\mathcal{L}_{cl}$ , confirming that the loss meaningfully improves visual coherence.

## 5. Conclusion

We introduce Chirpy3D, a novel framework for fine-grained 3D object generation in a zero-shot setting, leveraging only unposed 2D images from seen categories. Chirpy3D em-

ploy a multi-view diffusion model that decomposes objects into anchor parts in an unsupervised manner, representing both seen and unseen parts as continuous distributions. This formulation enables smooth interpolation and flexible part recombination, facilitating the synthesis of entirely new objects with species-specific details. Our experiments demonstrate that Chirpy3D outperforms existing methods in generating creative 3D objects with higher visual fidelity and fine-grained detail. Although our study focuses on birds, the framework is readily generalizable to other categories—such as dogs, quadrupeds, and character faces (see Figure 11). In all evaluated datasets, Chirpy3D effectively models part-based generation for any fine-grained collection. One potential application is in the gaming industry, where developers can significantly reduce coding efforts in character creation by leveraging Chirpy3D for automatic, flexible part-based synthesis. We believe Chirpy3D opens new possibilities for fine-grained 3D generation in various domains.

**Limitation.** The model’s generalizability is currently limited by constraints in the base model, particularly in multi-view consistency, controlling lighting and object poses. Another limitation is that the learned part latent codes are not fully disentangled as each code comprises both structural and texture information. Future work could focus on these to further broaden Chirpy3D’s versatility in generative 3D modeling.



## References

- [1] Omri Avrahami, Kfir Aberman, Ohad Fried, Daniel Cohen-Or, and Dani Lischinski. Break-a-scene: Extracting multiple concepts from a single image. In *SIGGRAPH Asia*, 2023. 1, 2
- [2] Yukang Cao, Yan-Pei Cao, Kai Han, Ying Shan, and Kwan-Yee K Wong. Dreamavatar: Text-and-shape guided 3d human avatar generation via diffusion models. In *CVPR*, 2024. 1
- [3] Mathilde Caron, Hugo Touvron, Ishan Misra, Hervé Jégou, Julien Mairal, Piotr Bojanowski, and Armand Joulin. Emerging properties in self-supervised vision transformers. In *ICCV*, 2021. 5, 6
- [4] Angel X Chang, Thomas Funkhouser, Leonidas Guibas, Pat Hanrahan, Qixing Huang, Zimo Li, Silvio Savarese, Manolis Savva, Shuran Song, Hao Su, et al. Shapenet: An information-rich 3d model repository. *arXiv preprint arXiv:1512.03012*, 2015. 2
- [5] Dongliang Chang, Yifeng Ding, Jiyang Xie, Ayan Kumar Bhunia, Xiaoxu Li, Zhanyu Ma, Ming Wu, Jun Guo, and Yi-Zhe Song. The devil is in the channels: Mutual-channel loss for fine-grained image classification. *TIP*, 2020. 2
- [6] Tianyi Chen, Yunfei Zhang, Xiaoyang Huo, Si Wu, Yong Xu, and Hau San Wong. Sphericgan: Semi-supervised hyper-spherical generative adversarial networks for fine-grained image synthesis. In *CVPR*, 2022. 2
- [7] Celia Cintas, Payel Das, Brian Quanz, Girmaw Abebe Tadesse, Skyler Speakman, and Pin-Yu Chen. Towards creativity characterization of generative models via group-based subset scanning. In *IJCAI*, 2022. 2
- [8] Payel Das, Brian Quanz, Pin-Yu Chen, Jae-wook Ahn, and Dhruv Shah. Toward a neuro-inspired creative decoder. In *IJCAI*, 2020. 2
- [9] Rui Ding, Kehua Guo, Xiangyuan Zhu, Zheng Wu, and Liwei Wang. Comgan: unsupervised disentanglement and segmentation via image composition. 2022. 2
- [10] Ruoyi Du, Dongliang Chang, Ayan Kumar Bhunia, Jiyang Xie, Zhanyu Ma, Yi-Zhe Song, and Jun Guo. Fine-grained visual classification via progressive multi-granularity training of jigsaw patches. In *ECCV*, 2020. 2
- [11] Ahmed Elgammal, Bingchen Liu, Mohamed Elhoseiny, and Marian Mazzone. Can: Creative adversarial networks generating "art" by learning about styles and deviating from style norms. In *ICCC*, 2017. 2
- [12] Rinon Gal, Yuval Alaluf, Yuval Atzmon, Or Patashnik, Amit H Bermano, Gal Chechik, and Daniel Cohen-Or. An image is worth one word: Personalizing text-to-image generation using textual inversion. *arXiv preprint arXiv:2208.01618*, 2022. 5, 12
- [13] Jun Gao, Tianchang Shen, Zian Wang, Wenzheng Chen, Kangxue Yin, Daiqing Li, Or Litany, Zan Gojcic, and Sanja Fidler. Get3d: A generative model of high quality 3d textured shapes learned from images. In *NeurIPS*, 2022. 2
- [14] Songwei Ge, Vedanuj Goswami, C. Lawrence Zitnick, and Devi Parikh. Creative sketch generation. In *ICLR*, 2021. 2
- [15] Kyle Genova, Forrester Cole, Daniel Vlasic, Aaron Sarna, William T Freeman, and Thomas Funkhouser. Learning shape templates with structured implicit functions. In *ICCV*, 2019. 2
- [16] Kyle Genova, Forrester Cole, Avneesh Sud, Aaron Sarna, and Thomas Funkhouser. Local deep implicit functions for 3d shape. In *CVPR*, 2020. 2
- [17] Yuan-Chen Guo, Ying-Tian Liu, Ruizhi Shao, Christian Laforte, Vikram Voleti, Guan Luo, Chia-Hao Chen, Zi-Xin Zou, Chen Wang, Yan-Pei Cao, and Song-Hai Zhang. threestudio: A unified framework for 3d content generation. <https://github.com/threestudio-project/threestudio>, 2023. 5, 14
- [18] Xiao Han, Yukang Cao, Kai Han, Xiatian Zhu, Jiankang Deng, Yi-Zhe Song, Tao Xiang, and Kwan-Yee K Wong. Headsculpt: Crafting 3d head avatars with text. In *Advances in Neural Information Processing Systems*, 2024. 1
- [19] Ju He, Shuo Yang, Shaokang Yang, Adam Kortylewski, Xiaoding Yuan, Jie-Neng Chen, Shuai Liu, Cheng Yang, and Alan Yuille. Partimagenet: A large, high-quality dataset of parts. *arXiv preprint arXiv:2112.00933*, 2021. 8
- [20] Amir Hertz, Or Perel, Raja Giryes, Olga Sorkine-Hornung, and Daniel Cohen-Or. Spaghetti: Editing implicit shapes through part aware generation. *TOG*, 2022. 2
- [21] Edward J Hu, Yelong Shen, Phillip Wallis, Zeyuan Allen-Zhu, Yanzhi Li, Shean Wang, Lu Wang, and Weizhu Chen. LoRA: Low-rank adaptation of large language models. In *ICLR*, 2022. 5, 12
- [22] Yukun Huang, Jianan Wang, Yukai Shi, Xianbiao Qi, Zheng-Jun Zha, and Lei Zhang. Dreamtime: An improved optimization strategy for text-to-3d content creation. *arXiv preprint arXiv:2306.12422*, 2023. 14
- [23] Ka-Hei Hui, Ruihui Li, Jingyu Hu, and Chi-Wing Fu. Neural template: Topology-aware reconstruction and disentangled generation of 3d meshes. In *CVPR*, 2022. 2
- [24] Yash Kant, Aliaksandr Siarohin, Ziyi Wu, Michael Vasilkovsky, Guocheng Qian, Jian Ren, Riza Alp Guler, Bernard Ghanem, Sergey Tulyakov, and Igor Gilitschenski. Spad: Spatially aware multi-view difusers. In *CVPR*, 2024. 1, 2

- [25] Bernhard Kerbl, Georgios Kopanas, Thomas Leimkühler, and George Drettakis. 3d gaussian splatting for real-time radiance field rendering. *ACM ToG*, 2023. 5
- [26] Xin Kong, Shikun Liu, Xiaoyang Lyu, Marwan Taher, Xiaojuan Qi, and Andrew J Davison. Eschnet: A generative model for scalable view synthesis. In *CVPR*, 2024. 2
- [27] Juil Koo, Seungwoo Yoo, Minh Hieu Nguyen, and Minhyuk Sung. Salad: Part-level latent diffusion for 3d shape generation and manipulation. In *ICCV*, 2023. 2
- [28] Jun Li, Zedong Zhang, and Jian Yang. Tp2o: Creative text pair-to-object generation using balance swap-sampling. In *ECCV*, 2024. 1, 2
- [29] Yuheng Li, Krishna Kumar Singh, Utkarsh Ojha, and Yong Jae Lee. Mixnmatch: Multifactor disentanglement and encoding for conditional image generation. In *CVPR*, 2020. 2
- [30] Yuheng Li, Krishna Kumar Singh, Yang Xue, and Yong Jae Lee. Partgan: Weakly-supervised part decomposition for image generation and segmentation. In *BMVC*, 2021. 2
- [31] Ruoshi Liu, Rundi Wu, Basile Van Hoorick, Pavel Tokmakov, Sergey Zakharov, and Carl Vondrick. Zero-1-to-3: Zero-shot one image to 3d object. In *ICCV*, 2023. 2
- [32] Ilya Loshchilov and Frank Hutter. Decoupled weight decay regularization. In *ICLR*, 2018. 12
- [33] B Mildenhall, PP Srinivasan, M Tancik, JT Barron, R Ramamoorthi, and R Ng. Nerf: Representing scenes as neural radiance fields for view synthesis. In *ECCV*, 2020. 5
- [34] Kam Woh Ng, Xiatian Zhu, Yi-Zhe Song, and Tao Xiang. Concepthash: Interpretable fine-grained hashing via concept discovery. In *CVPRW*, 2024. 2
- [35] Kam Woh Ng, Xiatian Zhu, Yi-Zhe Song, and Tao Xiang. Partcraft: Crafting creative objects by parts. In *ECCV*, 2024. 1, 2, 3, 4, 5, 7, 12
- [36] Amin Heyrani Nobari, Muhammad Fathy Rashad, and Faez Ahmed. Creativegan: Editing generative adversarial networks for creative design synthesis. *arXiv preprint arXiv:2103.06242*, 2021. 2
- [37] Jeong Joon Park, Peter Florence, Julian Straub, Richard Newcombe, and Steven Lovegrove. Deepsdf: Learning continuous signed distance functions for shape representation. In *CVPR*, 2019. 2
- [38] Ben Poole, Ajay Jain, Jonathan T Barron, and Ben Mildenhall. Dreamfusion: Text-to-3d using 2d diffusion. In *ICLR*, 2022. 5
- [39] Alec Radford, Jong Wook Kim, Chris Hallacy, Aditya Ramesh, Gabriel Goh, Sandhini Agarwal, Girish Sastry, Amanda Askell, Pamela Mishkin, Jack Clark, et al. Learning transferable visual models from natural language supervision. In *ICML*, 2021. 5
- [40] Elad Richardson, Kfir Goldberg, Yuval Alaluf, and Daniel Cohen-Or. Conceptlab: Creative generation using diffusion prior constraints. *arXiv preprint arXiv:2308.02669*, 2023. 1, 2
- [41] Joe Rocca. Sims4 faces. <https://huggingface.co/datasets/rocca/sims4-faces>, 2022. 8
- [42] Nataniel Ruiz, Yuanzhen Li, Varun Jampani, Yael Pritch, Michael Rubinstein, and Kfir Aberman. Dreambooth: Fine tuning text-to-image diffusion models for subject-driven generation. In *CVPR*, 2023. 5
- [43] Othman Sbai, Mohamed Elhoseiny, Antoine Bordes, Yann LeCun, and Camille Couprie. Design: Design inspiration from generative networks. In *ECCVW*, 2019. 2
- [44] Ruoxi Shi, Hansheng Chen, Zhuoyang Zhang, Minghua Liu, Chao Xu, Xinyue Wei, Linghao Chen, Chong Zeng, and Hao Su. Zero123++: a single image to consistent multi-view diffusion base model, 2023. 2, 14
- [45] Yichun Shi, Peng Wang, Jianglong Ye, Long Mai, Kejie Li, and Xiao Yang. Mvdream: Multi-view diffusion for 3d generation. In *ICLR*, 2023. 1, 2, 3, 5, 12, 15
- [46] Yawar Siddiqui, Antonio Alliegro, Alexey Artemov, Tatiana Tommasi, Daniele Sirigatti, Vladislav Rosov, Angela Dai, and Matthias Nießner. Meshgpt: Generating triangle meshes with decoder-only transformers. In *CVPR*, 2024. 2
- [47] Krishna Kumar Singh, Utkarsh Ojha, and Yong Jae Lee. Finegan: Unsupervised hierarchical disentanglement for fine-grained object generation and discovery. In *CVPR*, pages 6490–6499, 2019. 2
- [48] Jiayang Tang, Jiawei Ren, Hang Zhou, Ziwei Liu, and Gang Zeng. Dreamgaussian: Generative gaussian splatting for efficient 3d content creation. In *ICLR*, 2024. 5, 14
- [49] Yael Vinker, Andrey Voynov, Daniel Cohen-Or, and Ariel Shamir. Concept decomposition for visual exploration and inspiration. In *SIGGRAPH Asia*, 2023. 2
- [50] Catherine Wah, Steve Branson, Peter Welinder, Pietro Perona, and Serge Belongie. The caltech-ucsd birds-200-2011 dataset. 2011. 5
- [51] Xiu-Shen Wei, Yi-Zhe Song, Oisín Mac Aodha, Jianxin Wu, Yuxin Peng, Jinhui Tang, Jian Yang, and Serge Belongie. Fine-grained image analysis with deep learning: A survey. *TPAMI*, 2021. 2
- [52] Zhijie Wu, Xiang Wang, Di Lin, Dani Lischinski, Daniel Cohen-Or, and Hui Huang. Sagnet: Structure-

- aware generative network for 3d-shape modeling. *TOG*, 2019. [2](#)
- [53] Jiale Xu, Weihao Cheng, Yiming Gao, Xintao Wang, Shenghua Gao, and Ying Shan. Instantmesh: Efficient 3d mesh generation from a single image with sparse-view large reconstruction models. *arXiv preprint arXiv:2404.07191*, 2024. [7](#), [14](#)
- [54] Tao Xu, Pengchuan Zhang, Qiuyuan Huang, Han Zhang, Zhe Gan, Xiaolei Huang, and Xiaodong He. AttnGAN: Fine-grained text to image generation with attentional generative adversarial networks. In *CVPR*, 2018. [2](#)
- [55] Jing Yang, Kyle Fogarty, Fangcheng Zhong, and Cengiz Oztireli. Sym3d: Learning symmetric triplanes for better 3d-awareness of GANs. *arXiv preprint arXiv:2406.06432*, 2024. [2](#)
- [56] Taoran Yi, Jiemin Fang, Junjie Wang, Guanjun Wu, Lingxi Xie, Xiaopeng Zhang, Wenyu Liu, Qi Tian, and Xinggang Wang. Gaussiandreamer: Fast generation from text to 3d gaussians by bridging 2d and 3d diffusion models. In *CVPR*, 2024. [1](#)
- [57] Heliang Zheng, Jianlong Fu, Zheng-Jun Zha, and Jiebo Luo. Looking for the devil in the details: Learning trilinear attention sampling network for fine-grained image recognition. In *CVPR*, 2019. [2](#)

## A. Derivation

We use the symbol  $x$  to represent the part latent  $l$  for clarity. Assuming a multivariate Gaussian distribution with a spherical covariance matrix  $\sigma^2\mathbb{I}$ , the probability density function is expressed as:

$$p(\mathbf{x}) = \frac{1}{\sqrt{2\pi\sigma^2}} \exp\left(-\frac{\|\mathbf{x} - \boldsymbol{\mu}\|^2}{2\sigma^2}\right). \quad (9)$$

Since we assume a zero-mean Gaussian distribution, i.e.,  $bmmu = 0$ , the expression simplifies to:

$$p(\mathbf{x}) = \frac{1}{\sqrt{2\pi\sigma^2}} \exp\left(-\frac{\|\mathbf{x}\|^2}{2\sigma^2}\right). \quad (10)$$

Taking the logarithm of  $p(\mathbf{x})$  yields:

$$\log p(\mathbf{x}) = \log\left(\frac{1}{\sqrt{2\pi\sigma^2}}\right) + \left(-\frac{\|\mathbf{x}\|^2}{2\sigma^2}\right) \quad (11)$$

Maximizing  $\log p(\mathbf{x})$  is therefore equivalent to minimizing the term:

$$\mathcal{L}_{\text{reg}} = \frac{\|\mathbf{x}\|^2}{2\sigma^2} \quad (12)$$

In practice, we set  $\sigma^2 = 1$  for simplicity, leading to the regularization loss  $\mathcal{L}_{\text{reg}}$ .

## B. Implementation Details

### B.1. Settings

For finetuning MVDream, we select AdamW [32] as optimizer and learn at a constant learning rate of 0.0001 and weight decay of 0.01. We apply random horizontal flipping for data augmentation. Following MVDream [45], we train on images with resolution  $256 \times 256$ . We integrate the LoRA design [21] from `diffusers` library<sup>5</sup>, in which the low-rank adapters are added to the  $QKV$  and  $out$  components of all cross-attention modules. For attention loss  $\mathcal{L}_{\text{attn}}$ , we select cross-attention maps with feature map sizes of  $8 \times 8$  and  $16 \times 16$ , given input resolution of  $256 \times 256$ . For 3D generation described in Sec. 3.4 & Sec. 4.2, including generated objects in Fig. 1 and supplementary material, we build upon `MVDream-threestudio`<sup>6</sup>. The SDS loss  $\mathcal{L}_{\text{SDS}}$  used in our setup follows MVDream’s [45]  $x_0$ -reconstruction loss, with a CFG rescale of 0.3.

### B.2. Competitors

Table 5 shows the comparison of different methods in components.

<sup>5</sup>[https://github.com/huggingface/diffusers/blob/main/examples/text\\_to\\_image/train\\_text\\_to\\_image\\_lora.py](https://github.com/huggingface/diffusers/blob/main/examples/text_to_image/train_text_to_image_lora.py)

<sup>6</sup><https://github.com/bytedance/MVDream-threestudio>

Method	$\mathcal{L}_{\text{diff}}$	$\mathcal{L}_{\text{attn}}$	$\mathcal{L}_{\text{cl}}$	$\mathcal{L}_{\text{reg}}$	s	f	p	g	t
Textual Inversion [12]	✓	✓	✗	✗	✗	✗	✗	✗	✓
PartCraft [35]	✓	✓	✗	✗	✗	✗	✗	✓	✓
Chirpy3D	✓	✓	✓	✓	✓	✓	✓	✓	✗

Table 5. Comparison among Textual Inversion, PartCraft and Chirpy3D.  $s$  denotes species embeddings.  $f$  denotes mapping from species embedding to latent space.  $p$  is part latent space.  $g$  is projector from latent space to textual embedding.  $t$  is learnable textual embeddings. For Chirpy3D  $t$  is from  $g$  with input  $l$ . For PartCraft,  $t$  is from  $g$  with input  $t$ . For Textual Inversion, it optimizes  $t$ .

### Algorithm 1 Code snippet for diversity evaluation

```
# db_feats: DINO feats of training images (Nx768)
# query_feats: DINO feats of generated images (Qx768)
# db_labels: Training ground-truth labels (N)

def retrieve(query_features, db_features, db_labels):
    # both features assume normalized
    cossim = query_features @ db_features.t() # (Q, N)
    indices = torch.argsort(cossim, dim=-1)
    top5 = indices[:, :5]
    idx = torch.arange(len(db_features)).to(db_labels.device)
    return (
        db_labels[top5.reshape(-1)].reshape(top5.size(0),
        top5.size(1))
    )

def histogram_entropy(hist):
    # Normalize the histogram to obtain probabilities
    prob = hist / hist.sum()

    # Compute the entropy
    entropy = -torch.sum(prob * torch.log(prob))

    return entropy

retrieve_labels = retrieve(
    query_feats,
    db_feats,
    db_labels
)

hist1 = torch.zeros(200)
for i in range(200):
    hist1[i] = (retrieve_labels == i).sum()

entropy_hist1 = histogram_entropy(hist1)
print(f"Entropy_{n}:", entropy_hist1.item())
print("Num_classes", torch.exp(entropy_hist1).item())
```

### B.3. Algorithms

For the evaluation algorithm, please refer to Algorithm 1.

## C. Ablation Study

**Weights for  $\mathcal{L}_{\text{cl}}$ .** We set  $\lambda_{\text{cl}} \leq 0.001$ , as higher values degrade generation quality, often causing failures in object generation. See Figure 13.

**Dimension of  $D_l$ .** Table 6 presents a comparison of different variants with varying  $D_l$  dimensions. We choose  $D_l = 4$  as the default setting, as it achieves highest diversity in random sampling.

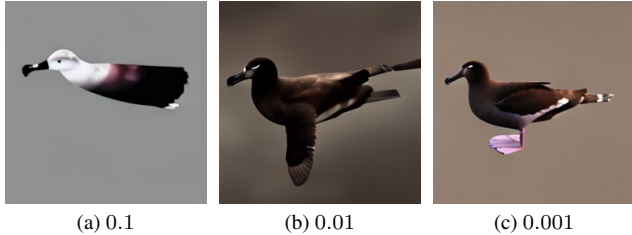


Figure 13. Comparison of generated images with different scales,  $\lambda_{cl}$ , for  $\mathcal{L}_{cl}$ .

$D_l$	4	16	32	64
$H$	<b>4.81</b>	4.68	4.67	4.33
$e^H$	<b>123.2</b>	108.1	106.7	76.3

Table 6. Entropy  $H$  and the effective number of classes  $e^H$  of Top-5 retrieved classes using generated images from random part latents. Higher values indicate greater diversity.



Figure 14. Image reconstruction from part latent inversion. We run 1,000 learning steps for optimization.

## D. Further Analysis

**Inversion experiment.** Once trained, we can perform part code inversion on input images, and use the learned part code to reconstruct original images. Figure 14 shows the visual comparison among three methods. Textual Inversion struggles with texture quality. PartCraft exhibits artifacts, possibly due to the ambiguity of input samples (e.g., camouflage birds). In contrast, our method successfully reconstructs the input with accurate size and significantly improved texture quality.

**Effect of  $\mathcal{L}_{attn}$ .** Figure 15 shows the visualization of the averaged cross-attention maps from multi-view images. Although we fine-tune MVDream exclusively on 2D images, it successfully transfers to multi-view image generation,

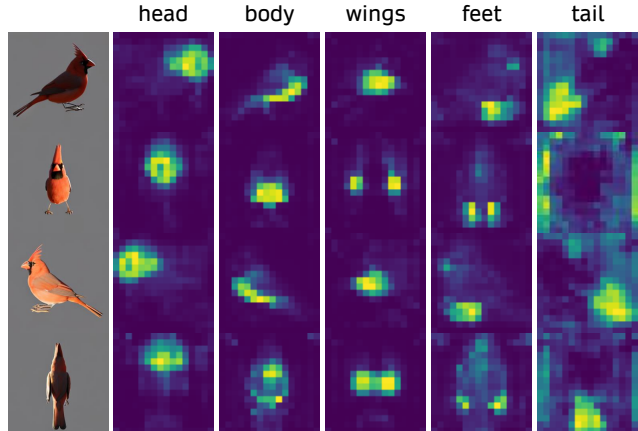


Figure 15. Visualization of cross-attention maps (averaged over all layers with size  $16 \times 16$ .) of multi-view images.

leveraging its learned prior. The cross-attention map highlights a strong correlation between the image and the tokens of the corresponding parts, demonstrating clear disentanglement—each part avoids attending to incorrect spatial locations, thanks to the part attention loss. Furthermore, when parts of the image are occluded (e.g., the tail is occluded when facing forward), the model attends to the background rather than incorrectly focusing on other parts.

	Textual Inversion	PartCraft	Chirpy3D (Ours)
1 - IoU	0.744	0.954	<b>0.957</b>

Table 7. Overlapping score between the cross-attention map of all parts.

**Analysis of part disentanglement.** In Table 7, we present the overlap score, defined as  $1 - \text{IoU}$  (intersection-over-union), calculated between the cross-attention maps of all parts (see an example in Fig. 15). The scores are averaged over 1,000 samples. These results demonstrate that the parts are effectively disentangled during generation using our Chirpy3D, enabling part-aware generation. In contrast, Textual Inversion struggles with part-aware generation, possibly because the learned word embeddings for each part are independent and lack mutual awareness, making it difficult to generate a cohesive whole object from individual parts.

We display the part latent space in Figure 16. In this latent space, we can traverse to sample desired species/generations. For instance, we can perform interpolation between two species, randomly sample, and also perform part composition, all can be done within this part latent space.

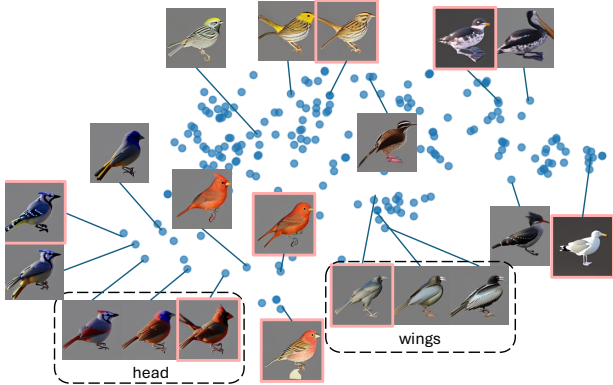


Figure 16. Visualizing part latent space via t-SNE embeddings.

## E. Different representations for 3D object Generation

### E.1. NeRF recipe

For NeRF-based 3D generation, we use `threestudio` [17] as our framework and `MVDream-threestudio` as a plugin. We implement a custom prompt processor to handle the input prompt, as we replace the word embeddings using Eq.2. After tokenization and before passing the word embeddings, we substitute the placeholder’s word embedding with our computed word embedding,  $t$ . An example prompt with placeholders is formatted as “a [part<sub>1</sub>] ... [part<sub>M</sub>] bird.”

We use all default settings, except for setting the number of samples per ray to 256 to prevent out-of-memory errors and disabling background color augmentation.

The guidance scale is set to 7.5 by default. Different timesteps affect the SDS optimization process [22]. Lower timesteps (less noise) emphasize detailed textures, while higher timesteps (more noise) focus on coarse structure. During SDS loss optimization, the timestep is randomly sampled within a specified minimum and maximum range.

We set the minimum timestep range to decay from 0.98 to 0.02 over 3,000 steps and the maximum timestep range to decay from 0.98 to 0.3 over 8,000 steps. We observe that bird structures begin forming around 1,000 steps. Therefore, we quickly decay the minimum timesteps to 0.02 to allow the model to focus on texture details during the early stages of training.

### E.2. 3DGS recipe

For 3DGS-based generation, we use DreamGaussian’s [48] official implementation, with the training strategy used in NeRF recipe.

Figure 17 shows that our Chirpy3D can be used in both NeRF and 3DGS-based 3D generation.

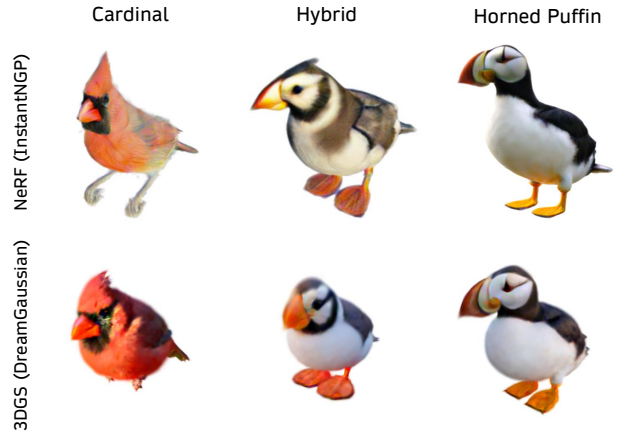


Figure 17. Optimization-based 3D generation with NeRF or 3DGS.

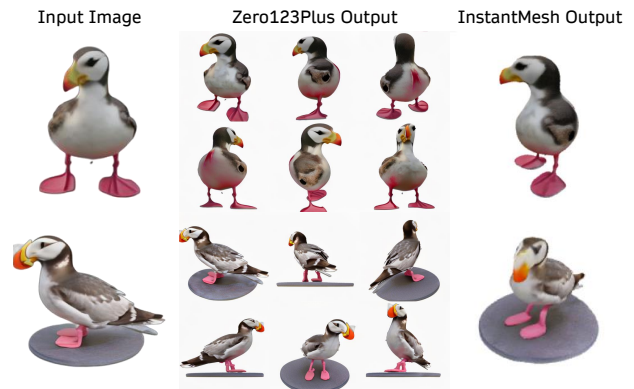


Figure 18. Image-to-3D using front view and side view of generated object.

### E.3. InstantMesh

We also present additional results in Figure 18, where generated images are processed through InstantMesh [53] to directly obtain 3D objects. While it provides fast inference, it occasionally produces incorrect conversions as it relies on Zero123Plus [44] to predict six views. This limitation arises because Zero123Plus may not have encountered the specific object (or similar objects) during training, leading to inaccurate view predictions. Fine-tuning an image-to-multi-view model typically requires 3D ground-truth data, which is why we focus on text-to-multi-view generation for fine-grained 3D generation. However, with the 3D objects obtained through our method, it may be possible to fine-tune an image-to-multi-view model without relying on 3D ground-truth data—an avenue worth exploring in future research.

## F. Multi-view generation on common token and fine-grained token



(a) a bird, 3d asset.



(b) a cardinal, 3d asset.

Figure 19. Multi-view generation with text prompt through MVDream [45]. The guidance scale is 7.5. Each row is a different seed. **(a)** The generation varies for different seeds for the token “bird”. **(b)** The generation with a fine-grained token “cardinal”. As highly similar objects are generated for each seed, we can use a lower guidance scale for SDS loss and enable 3D generation without oversaturated effect.

## G. Multi-view generation on existing species



Figure 20. Multi-view generation on existing species, trained with respective methods (a, b, c). (d) One of the training images of the species. Not only our Chirpy3D (c) can reconstruct well in multi-view perspective comparing to Textual Inversion (a) and PartCraft (b), but our generated images are also consistent in terms of orientation and cleaner background.



## H. Multi-view generation on novel species (random sampling)



Figure 21. Multi-view generation on novel species (random sampling), trained with respective methods. All were generated with the same seed but with different sampled part latents. (a) Trained with Textual Inversion, the generated images are often incomprehensible, indicating that direct sampling from word embedding space is insufficient to generate novel species. (b) PartCraft has a non-linear projector to project word embeddings, while able to generate comprehensible objects, but lacking diversity since it is not trained to have a continuous distribution of part latents. (c) Our Chirpy3D not only can generate images of diverse species, also stable in terms of bird pose.

## I. Multi-view generation on novel species (interpolation)



Figure 22. Multi-view generation on novel species (interpolation) trained with respective methods. All images were generated using the same seed, but with different interpolated part latents. **(a)** Trained with Textual Inversion, the generated images are often incomprehensible, consistent with previous visualizations. **(b)** PartCraft exhibits an abrupt switching effect, with the object remaining unchanged before and after switching, as it is not designed to support a continuous distribution of part latents. **(c)** Our Chirpy3D method successfully generates smooth interpolated samples.

## J. Qualitative comparisons of visual coherency before and after applying feature consistency loss

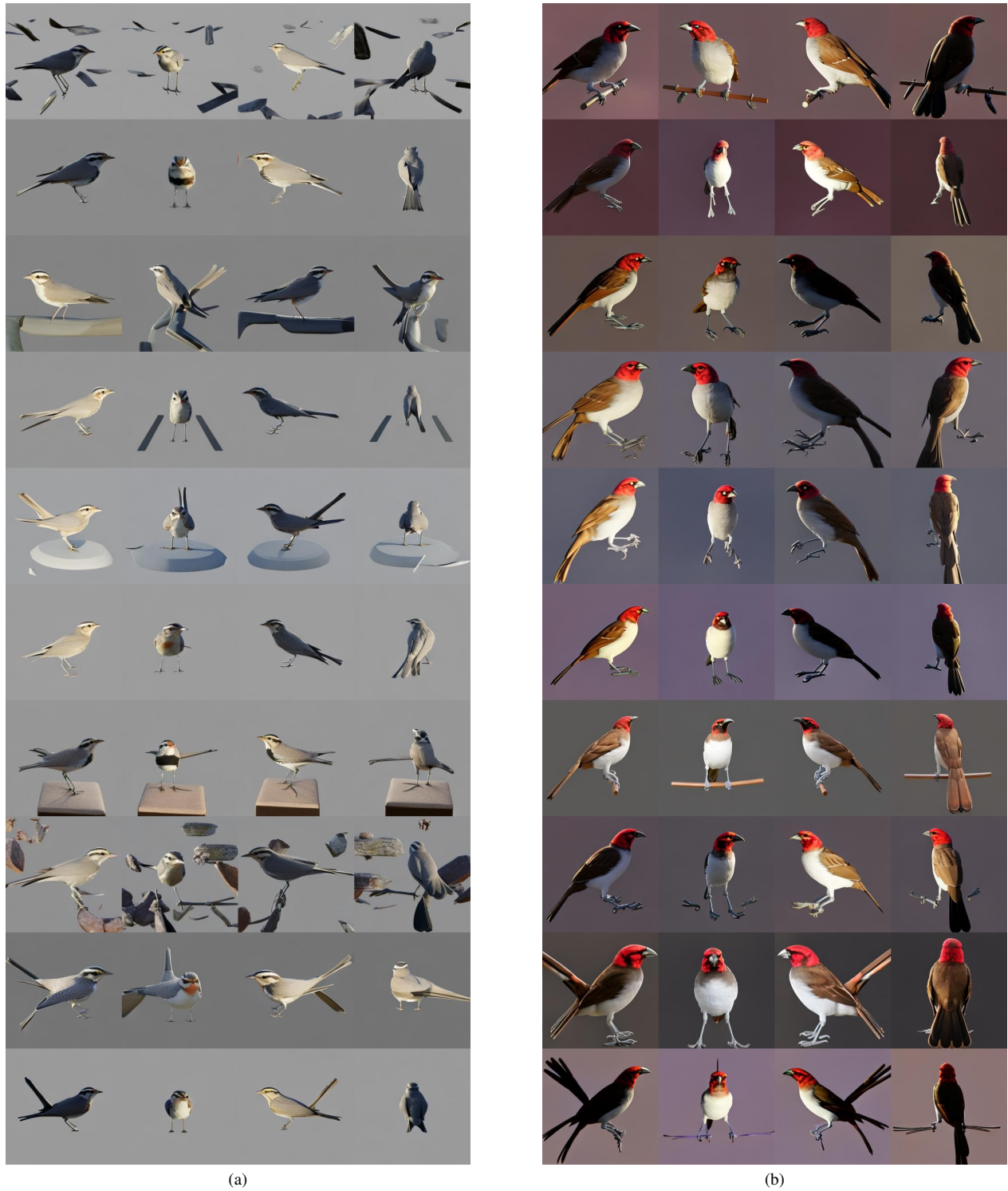


Figure 23. Each row is a different seed with a random sampled part latents (a) before applying  $\mathcal{L}_{ci}$  and (b) after applying. We can see that, although the part latents are unseen during training, applying the loss can increase visual coherency and less artifacts.